Aerosol and Air Quality Research, 12: 1444–1458, 2012

ISSN: 1680-8584 print / 2071-1409 online
doi: 10.4209/aaqr.2012.01.0005

Aerosol Features during Drought and Normal Monsoon Years: A Study Undertaken with Multi-Platform Measurements over a Tropical Urban Site

K. Vijayakumar, P.C.S. Devara*, C.P. Simha

Indian Institute of Tropical Meteorology, Dr. Homi Bhabha Road, Pune 411 008, India

ABSTRACT

This paper reports the results of aerosol optical characteristics over a tropical urban station at Pune, India, during drought and normal monsoon years, based on ground-based and satellite observations for the period 2008–2010. Ground-based data from MICROTOPS-II and AERONET, and satellite data products from Moderate Resolution Imaging Spectroradiometer (MODIS) and Ozone Monitoring Instrument (OMI) sensors, were utilized in the study. Detailed analysis of this data revealed that the maximum values of aerosol optical depth (AOD) and minimum values of precipitable water content (PWC) were observed during a drought year (2009) compared to normal monsoon years (2008 and 2010). In order to characterize aerosols further, the Ångström parameters α and β were evaluated. Using the least squares method, α is calculated in the spectral interval of 380–1020 nm, along with the coefficients a_1 and a_2 of the second-order polynomial fitted to the plotted logarithm of AOD versus the logarithm of wavelength. Meteorological parameters, such as temperature and relative humidity, have been measured during the course of the study, as well as the variations in monthly rainfall over the experimental site. The high surface temperatures and low rainfall amounts during the pre-monsoon and monsoon seasons of 2009 lead to an increase in AOD as compared to those in 2008 and 2010. The ground-based observations from MICROTOPS-II reveal good correlation with satellite observations of the MODIS and OMI sensors, and also correlate with the AERONET observations, corroborating the results. Discrimination of aerosol types from radiometric measurements and the tropospheric circulation obtained from the NCEP/NCAR (National Centers for Environmental Prediction/National Center for Atmospheric Research) reanalysis were also discussed, and found to be consistent.

Keywords: MICROTOPS-II; AOD; Ångström parameters; Rainfall.

INTRODUCTION

Atmospheric aerosols from natural and anthropogenic sources have great importance because they scatter and absorb solar and terrestrial radiation, involving in the formation of clouds and precipitation as cloud condensation and ice nuclei, and change the microphysical structure and possibly the lifetime of clouds within the atmosphere (Haywood and Boucher, 2000; Bellouin *et al.*, 2005; Rosenfeld *et al.*, 2006). To understand the effects of aerosols on our geo-biosphere systems, it is essential to characterize their optical, physical, and chemical properties at different locations because of the regional heterogeneity of their properties and their short lifetime (Satheesh *et al.*, 2002). The life time of aerosols is mainly determined by the size range of particles. It also depends on external factors such as wind and rain. Optical properties of aerosols can vary greatly depending on environmental conditions as well as on local sources. Moreover, these properties depend on the aerosol size distribution as well as on the refractive index and total atmospheric loading. This results in attenuation or extinction of solar radiation reaching the earth`s surface (Ranjan *et al.*, 2007).

The distribution of atmospheric aerosol optical depth (AOD) is influenced by both surface and atmospheric conditions. Asia is the most prominent monsoon region (Wang, 2006); the monsoon circulation as a large dynamical system occurs over southern and eastern Asia. The monsoon circulation may influence the spatial and temporal variation patterns of aerosol loading. For example, Bao *et al.* (2008) using rotated principal component analysis showed that the spatial and temporal characteristics of the AOD over eastern Asia were closely associated with wind fields. Statistical analyses on the Moderate Resolution Imaging Spectroradiometer (MODIS) data proved that wind direction is responsible for the observed negative and positive AOD anomalies, corroborating the negative and positive rainfall anomalies observed over the Arabian Sea in July (Rahul *et al.*, 2008). Li and Ramanathan (2002) used 5 years of satellite-derived AOD data to document the large seasonal

* Corresponding author. Tel.: +91-20-25904251;
Fax: +91-20-25865142
E-mail address: devara@tropmet.res.in

variations in the AOD modulated by the monsoons. Badarinath *et al.* (2007a) have studied on multiyear ground-based and satellite observations of aerosol properties over a tropical urban area in India during 2003–2005. It is found that AOD concentrations at shorter wavelengths were high during drought year 2004 compared to normal years 2003 and 2005, suggesting increased loading of fine-mode particles over a tropical urban area in India and higher incidence of fires during 2004 over the Indian region compared to other years. This is reflected in higher AOD values observed during 2004. Recently, Bhawar and Devara (2010) worked extensively on successive contrasting monsoons 2001–2002 in terms of aerosol variability over Pune, India and pointed out that the higher AODs and less precipitation was observed in drought year 2002 compared to active monsoon year 2001. Rahul *et al.* (2011) have also reported the interface between absorbing aerosols and droughts.

A wide variety of aerosol, ozone and water vapor products have been routinely measured using a ground-based, MICROTOPS II (covering from UV to NIR wavelength region) at the Indian Institute of Tropical Meteorology (IITM), Pune (Lat. 18°32'N, Long. 73°51'E, Altitude 559 m), India (Dani *et al.*, 2010). These products include column-integrated aerosol optical depth (AOD), ozone (TCO) and precipitable water content (PWC). In this communication, we present the results of the synthesis of this extensive database, focusing on the spatial and temporal variations in aerosol properties and association with synchronous satellite measurements during 2008–2010. Temporal variation of Ångström exponent and turbidity coefficient and also discrimination of aerosol types are studied. NCEP/NCAR reanalysis winds are discussed.

EXPERIMENTAL STATION AND METEOROLOGY

The experimental station of Pune is situated on the lee-side of the Western Ghats and is about 100 km inland from the west coast of India. Observations were carried out on the terrace of the building at about 10 m above the surface, at the Indian Institute of Tropical Meteorology, Pune. The environment in the immediate vicinity of the station is urban, with several small industries nearby, and the possible aerosol type present over the station is a mixture of water-soluble, dust-like and soot-like aerosols (Khemani, 1989). Soil dust is the major source of aerosols present over the experimental station (Khemani *et al.*, 1985; Praveen, 2008). Formation of aerosols in the accumulation mode is considered to be due to gas-to-particle conversion processes, whereas coarse aerosols are attributed mainly to wind-blown dust (Khemani *et al.*, 1982). The site is surrounded on all sides by hillocks of variable heights (up to 200 m), forming a valley like appearance. Brick kilns are situated at a distance of about 1 km to the west of observational site.

The weather at the experimental site during the pre-monsoon season (March–May) is very hot with mostly gusty surface winds and the daytime maximum temperature reaching around 40°C. During this season the dust content in the atmosphere is at a maximum, and cumulonimbus-type cloud development takes place around late afternoon to evening (Khemani *et al.*, 1982; Khemani, 1989). Development of low pressure system due to increased heating over land starts over India in the pre-monsoon, when all over India has the same pressure distribution. The air flow in the lower troposphere is predominantly westerly during the south-west (SW) monsoon season (June–September), which brings a large influx of moist air from the Arabian Sea. The region receives light, continuous or intermittent rain, and the atmosphere is relatively free from dust during this season. The westerly flow sets in during the post-monsoon season (October–November). The continental air masses, rich in nuclei of continental origin, pass over the region during this season. The daily minimum temperature falls very rapidly by the end of October. Fair-weather conditions, with clear skies and very low relative humidity, exist during the winter (December–February) season. Low-level inversions during the morning and evening hours, and dust haze during the morning hours, occur during this season.

METHODOLOGY

MICROTOPS-II

The MICROprocessor-controlled Total Ozone Portable Spectrometer (MICROTOPS-II) was used to measure the aerosol optical depth (AOD) at the wavelengths 380, 440, 500, 675, 870 and 1020 nm (Morys *et al.*, 2001) as well as the total column ozone (TCO) and precipitable water content (PWC), which were operated every 10–30 min from sunrise to sunset period. The sun photometer works on the principle of measuring the solar radiation intensity at some specified wavelengths and converts it to optical depth by knowing the corresponding intensities at the top of the atmosphere (TOA). The TOA irradiance at each wavelength was calculated via the well-known Langley method. For this, the expression given by Kasten and Young (1989) for the air mass computation was used. The instrument measures the irradiance signals at different wavelengths in mV, from which the absolute irradiance in Wm^{-2} is obtained by multiplying the signal with calibration factor (Wm^{-2}/mV). The calibration relies on a high-performance voltage reference with the temperature coefficient $\leq$ 0.001% per degree Celsius and long-term stability of ~0.005% per year. The full width at half maximum bandwidth at each of these wavelength channels is 2.4 ± 0.4 nm, and the accuracy of the sun-targeting angle is better than 0.1°. In order to avoid any errors in sun-targeting angle, the MICROTOPS-II was mounted on a tripod stand throughout the experimental period. The whole procedure for the AOD derivation can be found in the literature (for example, Devara *et al.*, 2001; Badarinath *et al.*, 2007b).

CIMEL Sun-Sky Radiometer

The Sun-sky radiometer measurements reported in this paper were made with a CIMEL Electronique CE-318 instrument as a part of the AERONET global network. This instrument is described in detail in the work of Holben *et al.* (1998, 2001); however, a brief description highlighting the essential features is given here. The automatic-tracking Sun-sky scanning radiometers make direct Sun measurements with a 1.2° full field of view at

least every 15 min interval at 440, 675, 870, 940, and 1020 nm (nominal wavelengths), in addition to three polarized channels at 870 nm. The direct Sun measurements take 8 sec to scan all eight wavelengths, with a motor-driven filter wheel positioning each filter in front of the detector. A sequence of three measurements (termed a triplet) taken 30 s apart are made resulting in three measurements at each wavelength within a 1 min period. These solar extinction measurements are then used to compute aerosol optical depth at each wavelength except for the 940 nm channel, which is used to retrieve precipitable water vapor in centimeters. The spectral AOD data have been screened for clouds following the methodology of Smirnov *et al.* (2000), which relies on the greater temporal variance of cloud optical depth versus aerosol optical depth.

Ångström Coefficients α and β

The spectral dependence of the AOD was used in this work to compute the Ångström's exponent "α". A spectrally-averaged value of this exponent, which contains information about the size of the particles or the volume fraction of the fine versus coarse-mode particles (Schuster *et al.*, 2006), can be obtained by fitting the Ångström's formula (Ångström *et al.*, 1964):

$$AOD_\lambda = \beta\lambda^{-\alpha} \quad (1)$$

where AOD_λ is the estimated AOD at the wavelength λ, β is the Ångström's turbidity coefficient which equals AOD at λ = 1 μm, and the wavelength exponent α is a good indicator of the fraction of accumulation mode particles (r < 1 μm) to coarse-mode particles (r >1 μm). Although in definition α is assumed independent to the wavelength, it is well known that α depends on λ (Kaskaoutis *et al.*, 2009). The Ångström formula is a special case of a more complicated equation valid for a limited range of particle diameters and a limited interval of wavelengths. The validity of this theory presupposes that the Junge power-law is valid for the particle-radius range, where significant extinction takes place and that the spectral variation of the refractive index does not impose significant variations on the Mie extinction factor (Kaskaoutis *et al.*, 2006). Taking the logarithms of both sides of Eq. (1) obtains:

$$\ln AOD_\lambda = -\alpha \ln\lambda + \ln\beta \quad (2)$$

A more precise empirical relationship between aerosol extinction and wavelength is obtained with a second-order polynomial fit (Eck *et al.*, 1999, 2001a; Pedros *et al.*, 2003; Kaskaoutis and Kambezidis, 2006) as

$$\ln AOD_\lambda = a_2 (\ln\lambda)^2 + a_1 \ln\lambda + a_o \quad (3)$$

where the coefficient "a_2" accounts for a curvature often observed in sun-photometry measurements. This curvature can be an indicator of the aerosol-particle size, with negative curvature indicating aerosol-size distributions dominated by fine-mode and positive curvature indicating size distributions with significant contribution by the coarse-mode aerosols (Schuster *et al.*, 2006).

The spectral variation of Ångström exponent is commonly referred to as curvature; and the spectral curvature provides additional information on aerosol size distribution. The negative curvatures favor high fine volume fractions and positive curvatures favor low fine volume fractions at the intermediate values of alpha. Thus, the presence of curvature can be used to improve the assessment of aerosol size distributions at intermediate Ångström exponents (alpha values between 1 and 2). Multi-wavelength Ångström exponents, covering broader wavelength region, provide more accurate results under low turbidity conditions.

In the present study, the values of α were computed in the wavelength interval 380–1020 nm, applying the least squares method to Eq. (2). The linear fit to the logarithmic function of Eq. (2) is the most precise method, although the results may also depend on the spectral interval considered (Pedros *et al.*, 2003; Kaskaoutis and Kambezidis, 2008). The second-order polynomial fit (Eq. (3)) was also applied to the AOD values at six wavelengths (380, 440, 500, 675, 870 and 1020 nm), although three of them are sufficient for this computation as indicated by Eck *et al.* (2001a). Although the polynomial fit to Eq. 3 is more precise than the linear fit to Eq. (2), large errors can appear especially under low turbidity conditions. These errors were found to be lower when the spectral interval 380–1020 nm is used instead of 380–870 nm. For this reason, the spectral range 380–1020 nm was used for the computation of α, a_1 and a_2.

MODIS Satellite Retrievals

The Moderate Resolution Imaging Spectroradiometer (MODIS) is a key instrument aboard the Terra (EOS AM) and Aqua (EOS PM) satellites. The MODIS sensor is onboard the polar orbiting NASA-EOS Terra and Aqua spacecrafts with equator crossing times of 10:30 and 13:30 Local Solar Time (LST), respectively (Levy *et al.*, 2007). Terra's orbit around the Earth is timed so that it passes from north to south across the equator in the morning, while Aqua passes south to north over the equator in the afternoon. Because of the difference in direction, mid-latitude time differences between Terra and Aqua are approximately 1.5 hours in the Northern Hemisphere and 4.5 hours in the Southern Hemisphere (Kaufman *et al.*, 2005). MODIS acquires daily global data in 36 spectral bands from visible to thermal infrared (29 spectral bands with 1-km, 5 spectral bands with 500-m and 2 spectral bands with 250-m, nadir pixel dimensions) ranging from 0.4 to 14.4 μm. Numerous parameters describing various properties of physical features on land and ocean surfaces as well as in the atmosphere are retrieved operationally from MODIS data at different spatial and temporal resolutions. Several aerosol parameters are retrieved at 10-km spatial resolution from MODIS daytime data. The MODIS aerosol algorithm has two components, one adapted for retrieval over land (Kaufman *et al.*, 1997), and the other for retrieval over ocean (Tanré *et al.*, 1997) surfaces, because of the inherent differences in the solar spectral radiance interaction with these surfaces. The parameters retrieved include: aerosol optical depth (AOD) at several wavelengths (λ) and Ångström exponent (α) over

land and ocean; and effective radius (r_{eff}), and the proportion of AOD contributed by the small mode aerosols over ocean. To assess the quality of these parameters, a substantial part of the Terra-MODIS aerosol products acquired in 2000 have been validated globally and regionally, as reported by Chu *et al.* (2002), Ichoku *et al.* (2002) and Remer *et al.* (2005). In this study, the Terra and Aqua MODIS Level 3 (spatial resolution 1° × 1°) products are obtained from Giovanni website (http://gdata1.sci.gsfc.nasa.gov/daac-bin/G3/gui.cgi?instance_id=MODIS_DAILY_L3) during 2008–2010.

NCEP/NCAR Reanalysis Data

The NCEP/NCAR (National Centers for Environmental Prediction/National Center for Atmospheric Research) reanalysis wind field indicates that the atmospheric circulation, especially the horizontal wind convergence is the major factor that guides the formation and dynamics of the cluster. The surface flow patterns obtained from NCEP/NCAR reanalysis (http://www.cdc.noaa.gov) (Kalnay *et al.*, 1996) have been used to ascertain the synoptic meteorological conditions and source variability to the observation site during 2008–2010. The NCEP reanalysis provides long time series of gridded atmospheric and surface fields. The most reliable fields such as pressure heights, tropospheric temperature and specific humidity are obtained by merging short-term atmospheric forecasts with observations. NCEP fields are available from 1948, but since 1979, corresponding to the advent of new generation satellite data streams, the fields are of higher quality (Rawlins *et al.*, 2009). In addition, the meteorological data such as air temperature, relative humidity and rainfall datasets were collected from the India Meteorological Department (IMD), Pune and analyzed.

DISCUSSION

Monthly Variation in Aerosol Optical Depth (AOD)

Fig. 1 shows spectral variations of monthly mean AOD during 2008–2010, measured using Microtops–II Sunphotometer over the study area. The gaps in the datasets are due to unfavorable sky conditions during the south-west monsoon months. It can be seen from Fig. 1 that AOD values are higher during 2009 compared to other years, suggesting an additional loading of aerosols over the region. Higher concentrations of aerosol loading during the summer period could be attributed to the increased concentration of continental aerosol loading due to high temperatures in the study region, as well as other sources such as long-range transport of dust from west of the Arabian Sea (Devara *et al.*, 2002; Sumit *et al.*, 2011). In winter, strong nocturnal inversions are frequent, and whatever aerosols due to various human activities (domestic cooking, vehicular emissions, industrial emissions, etc.) are let out into the surface layer get trapped in the lower atmosphere due to less ventilation. Also, due to calm wind conditions, aerosols of soil-dust type are less during winter. Monthly mean AODs during the transition period of October–November (post-monsoon) are slightly less in magnitude at all wavelengths compared to that in the pre-monsoon and winter periods. The spectral variations of AOD during different seasons of 2008, 2009 and 2010 are presented in Table 1. Most of the aerosol load that gets into the atmosphere during the pre-monsoon is removed by rain-washout and cloud-scavenging processes during the summer monsoon (rainy) season.

Monthly Variation in Precipitable Water Content (PWC)

Monthly variations in PWC during 2008–2010 are shown in Fig. 2. PWC is high in summer and low in winter, as expected. Comparison between Figs. 1 and 2 reveals a correspondence between AOD and PWC, which suggests the growth of aerosol particles associated with higher PWC values. Such an association has already been reported by Gupta *et al.* (2003) and Pandey *et al.* (2004). Raj *et al.* (2008) studied temporal variations in sun photometer measured PWC in near IR band and its comparison with model estimates at a tropical Indian station and found the PWC during May 1998–May 2006 was about 1.32 cm, which was consistent with the present value of about 1.57 cm. Recently, Sumit *et al.* (2011) have studied the annual mean PWC over the Pune region using the CIMEL sun-sky radiometer. Their results show a mild increasing trend during 2004–

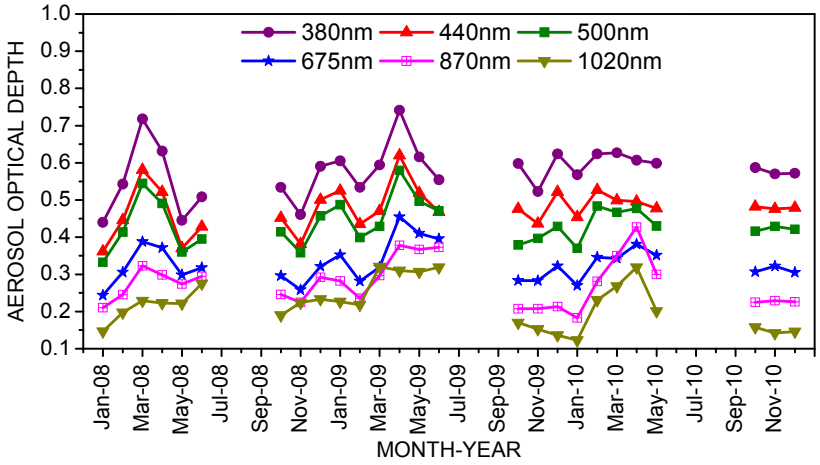

Fig. 1. Variation of aerosol optical depth (AOD) at different wavelengths during 2008–2010. Data gaps are due to unfavorable sky conditions.

Table 1. Seasonal variation of AOD at different wavelengths during 2008–2010.

Wavelength (nm)	Aerosol optical depth											
	2008			2009			2010					
	Winter	Pre-monsoon	Post-monsoon	Winter	Pre-monsoon	Post-monsoon	Winter	Pre-monsoon	Post-monsoon
380	0.52 ± 0.08	0.60 ± 0.14	0.50 ± 0.05	0.59 ± 0.05	0.65 ± 0.08	0.56 ± 0.05	0.59 ± 0.03	0.61 ± 0.01	0.58 ± 0.01
440	0.44 ± 0.07	0.49 ± 0.11	0.42 ± 0.05	0.49 ± 0.05	0.54 ± 0.08	0.46 ± 0.03	0.49 ± 0.04	0.49 ± 0.01	0.48 ± 0.00
500	0.40 ± 0.06	0.47 ± 0.09	0.39 ± 0.04	0.44 ± 0.04	0.50 ± 0.08	0.39 ± 0.01	0.43 ± 0.06	0.46 ± 0.02	0.42 ± 0.01
675	0.29 ± 0.04	0.35 ± 0.05	0.28 ± 0.03	0.32 ± 0.04	0.39 ± 0.07	0.28 ± 0.00	0.31 ± 0.04	0.36 ± 0.02	0.31 ± 0.01
870	0.25 ± 0.04	0.30 ± 0.02	0.24 ± 0.02	0.24 ± 0.04	0.35 ± 0.04	0.21 ± 0.00	0.23 ± 0.05	0.36 ± 0.06	0.23 ± 0.00
1020	0.19 ± 0.04	0.22 ± 0.00	0.21 ± 0.02	0.19 ± 0.05	0.31 ± 0.01	0.16 ± 0.01	0.17 ± 0.06	0.26 ± 0.06	0.15 ± 0.01

2009. The columnar PWC is observed to be smaller during 2009 in contrast to that during 2008 and 2010.

OMI and MICROTOPS Total Column Ozone (TCO) Variations

Ozone is an important trace gases that is being studied widely all over the world. In order to investigate the compatibility between the ozone variations obtained from ground-based and satellite techniques, MICROTOPS determined TCO values are compared with OMI derived values in Fig. 3. Both measurements show distinct annual oscillation with broad maximum during monsoon and minimum during winter months over this observing station which may allow the UV radiation to reach the surface. Thus, the agreement between these two techniques appears to be fairly good within the experimental limitations. An interesting feature is that both OMI and MICROTOPS exhibited lower ozone values during winter and pre-monsoon months and higher values during monsoon and post-monsoon seasons of 2009 compared to 2008 and 2010. The ground-based TCO values overestimate the OMI derived ozone. Such differences in TCO between MICROTOPS and OMI are considered to be due to large variability in the surface-level ozone concentration at the experimental location close to the urban site. Similar results have been reported for this experimental site by Raj *et al.* (2004) and Kalapureddy *et al.* (2008). Possible reasons for the discrepancy between satellite and ground-based measurements may be related to the instrument calibration and differences in the spatial resolution. In addition, temporal differences can also occur because of difference in timing as well as changes in atmospheric conditions. Further, MICROTOPS provides point observations as compared to about 125 × 100 km grid average values of OMI.

Albeit the summer peak does not show significant year-to-year change, the significant inter-annual variation during the winter-time minimum could be due to the influence of quasi-biennial oscillation in total ozone variations. A high-degree of year-to-year variability and largest absolute changes during the dynamically active winter and summer periods have been reported (WMO, 2003). Moreover, the height of the boundary layer or the mixing depth can significantly influence the dispersal of pollutants and ozone pre-cursor gases in the lower troposphere. Thus the lower mixing depth during monsoon and post-monsoon months and higher mixing depths during winter and pre-monsoon months could be responsible for the observed features. Raj *et al.* (2009) have studied the changes observed in sun photometer derived total column ozone and possible implications on surface-reaching UV radiation over Pune during May 1998–May 2003 and found the average value was 254 DU, which is consistent with that during 2008–2010 (286 DU). These changes are considered to be due to large-scale circulation-induced currents during monsoon over the experimental region.

The overall ozone concentration is found to be maximum in May. It decreases during monsoon and post-monsoon and reaches minimum in December. Thereafter, it gradually increases throughout the winter and reaches peak value in

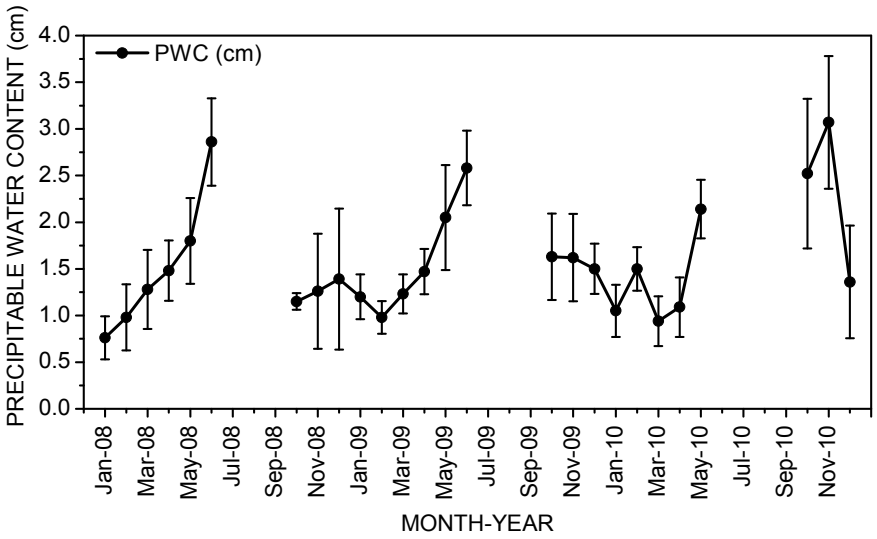

Fig. 2. Monthly variation in Precipitable Water Content.

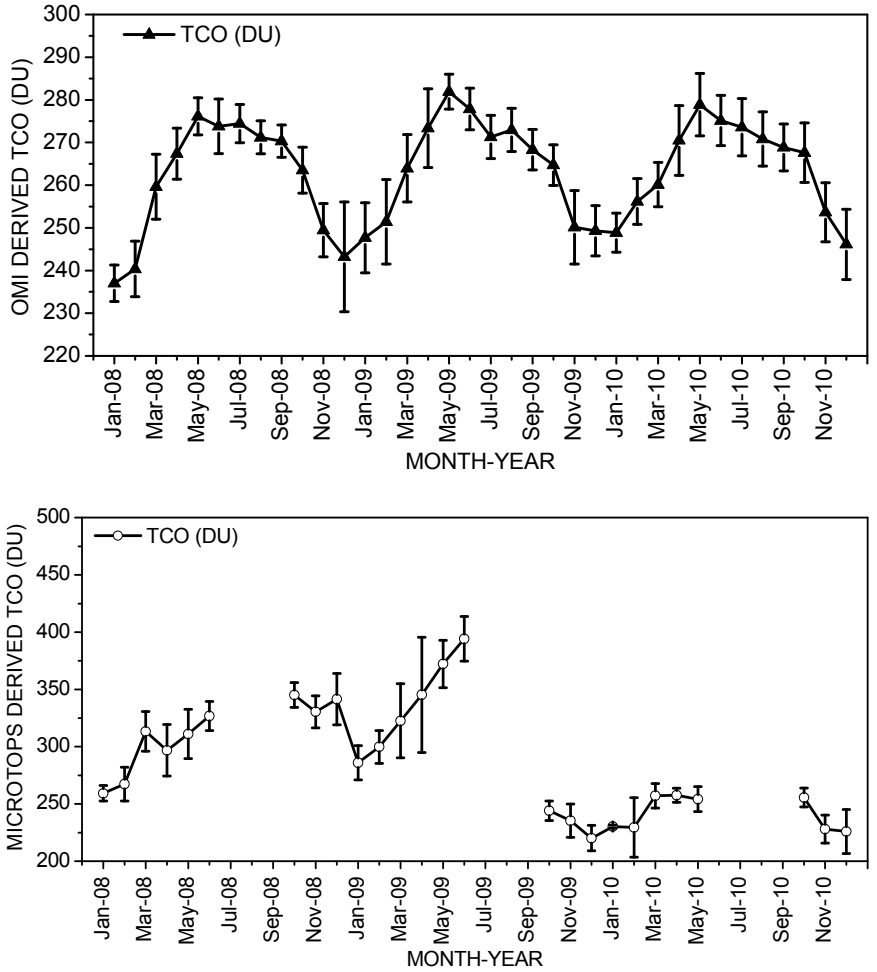

Fig. 3. Comparison between total column ozone (TCO) measured by the ground-based (MICROTOPS-II) and OMI satellite over Pune during 2008–2010.

summer. The primary cause of large values of ozone in May month may be due to the high solar flux acting upon a pool of accumulated NO_x and hydrocarbons built up during winter resulting in local photochemical production. Ozone is produced by photo-oxidation of pollutants (carbon mono-oxide and hydrocarbons) in the presence of adequate amount

of nitrogen oxides at lower altitudes. Once ozone is produced, it gets transported along with the wind, resulting in a high concentration in summer. During monsoon the pristine air from the Arabian Sea blows over Pune, resulting in a decrease in ozone concentration due to wash-out effects and transport of monsoon air masses.

Temporal Variations in Ångström Exponent and Turbidity Coefficient

The Ångström wavelength exponent (α), which represents the particle size distribution and the turbidity coefficient (β), which represents the aerosol loading have been derived and shown plotted in Fig. 4. It is evident from this figure that the values of alpha and beta are almost opposite to each other; implying higher values of beta are associated with smaller values of alpha, a fact that agrees with earlier studies by Bhawar (2008) and Dani *et al.* (2010).

The overall mean value of α at this urban location is 0.94, and the mean β is 0.23. It is also interesting to note that winter season mean α (1.11 ± 0.14) is higher than the pre-monsoon mean (0.78 ± 0.02). As a general rule, larger values of α indicate abundance of smaller-size particles, while smaller values indicate abundance of larger/coarse size particles. It can be seen from Fig. 4 that the average values of α are higher during October to February and lower during March to June. The maximum and minimum values of α vary between 1.45 ± 0.10 (December 2009, January 2010) and 0.47 ± 0.27 (April 2010). The maximum and minimum values of β vary between 0.33 ± 0.07 (June 2009) and 0.13 ± 0.01 (January 2010) at the observational site. Higher values of β are seen in the months of March, April, May and June indicate that the total aerosol mass loading is the highest during the pre-monsoon months. The relatively smaller values of α during winter and larger values of β during winter as compared to the pre-monsoon months in certain years are attributed partly due to intense haze formation due to elevated temperature inversions and associated trapping of local anthropogenic aerosols. As explained in the previous sections, over this station, fine-mode particles are more in the winter and coarse-mode particles of soil-dust origin are abundant during the pre-monsoon season. Added, the higher temperature associated with large-scale circulation features may have intensified this feature during 2009 as compared to that during 2008 and 2010. Thus, the results show the presence of more fine-mode particles in 2008 and 2010 than in 2009 suggesting greater loading of coarse-mode aerosols in 2009 as compared to that in 2008 and 2010 during pre-monsoon season.

Discrimination of Aerosol Types

In order to characterize the aerosol properties, data of both AOD and Ångström exponent values have to be used (Holben *et al.*, 2001) since they both strongly depend on wavelength. The AOD-α patterns have been utilized to describe different aerosol types (e.g., biomass smoke, anthropogenic aerosols, desert dust) at several locations (Eck *et al.*, 1999, 2001a, b; Masmoudi *et al.*, 2003; Kim *et al.*, 2004). Fig. 5 depicts the density maps of $AOD_{500\ nm}$ versus Ångström exponent (380–1020 nm) over the Pune region. These contour maps were constructed using 0.1 steps for both $AOD_{500\ nm}$ and $\alpha_{380–1020\ nm}$ values. In these maps, the rectangle areas denote urban/industrial (UI), clean maritime (CM), desert dust (DD) and mixed type (MT) aerosols, and boundaries of these areas correspond to the selected threshold values of $AOD_{500\ nm}$ and $\alpha_{380–1020\ nm}$. This method has been used in a number of studies (for example, Kalapureddy *et al.*, 2008 and references therein) and is based on the sensitivity of the two parameters to different, somewhat independent, microphysical aerosol properties; the Ångström exponent depends on particle size distribution (aerosol type), while the $AOD_{500\ nm}$ depends mainly on the aerosol column density. Therefore, the $AOD_{500\ nm}$ versus $\alpha_{380–1020\ nm}$ plot qualitatively indicates the amount and dimension of the observed aerosols.

In the present study, during 2008–2010, the $AOD_{500\ nm}$ ranges from 0.13 to 0.77 and the $\alpha_{380\text{-}1020\ nm}$ spans between 0.32 and 1.72. Therefore, the threshold values must be slightly changed from those utilized by Pace *et al.* (2006)

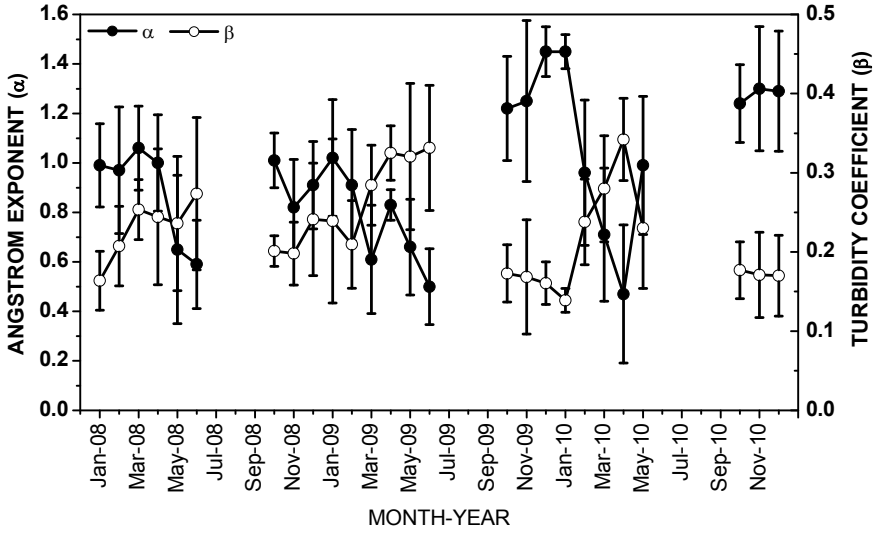

Fig. 4. Temporal variation of Ångström exponent and turbidity coefficient from January 2008 to December 2010.

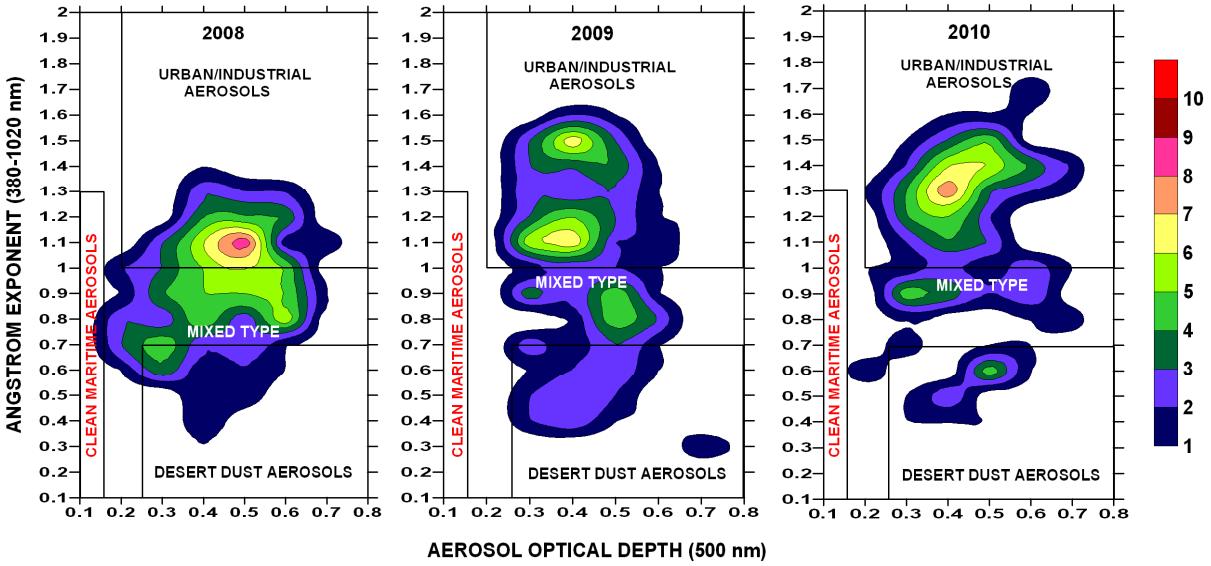

Fig. 5. Contour density maps of the Ångström exponent (380–1020 nm) versus aerosol optical depth (500 nm).

for Lampedusa. Therefore (i) values of $AOD_{500\ nm} < 0.15$ with $\alpha_{380–1020\ nm}$ values < 1.3 represent clean maritime aerosols, (ii) $AOD_{500\ nm} > 0.2$ and $\alpha_{380–1020\ nm} > 1.0$ can be used to characterize long-range transported UI aerosols, and (iii) $AOD_{500\ nm}$ values > 0.25 associated with $\alpha < 0.7$ are indicative of DD particles transported over oceanic areas. Finally, the remaining gaps reveal where the aerosols are difficult to be discriminated and they are considered as MT, bearing in mind the different effects of various aerosol-mixing processes in the atmosphere (e.g., coagulation, condensation, humidification, gas-to-particle conversion).

It is clear from Fig. 5 that, during 2008, the maximum density area is observed for the pair ($AOD_{500\ nm}$, $\alpha_{380–1020\ nm}$) = (0.5, 1.1) indicative of UI aerosols. This clearly indicates the influence of the anthropogenic pollution from the industrialized areas of the Indian west coast, which was found to have a spatial offshore extent of < 100 km at the coast (Moorthy *et al.*, 2008). But in 2009, two maximum density areas are observed. The primary density area is observed for the pair ($AOD_{500\ nm}$, $\alpha_{380–1020\ nm}$) = (0.4, 1.5) and secondary maximum density area is found for $AOD_{500\ nm}$ between 0.35 and 0.41; and $1.19 < \alpha_{380–1020\ nm} < 1.12$, both indicative of the presence of UI aerosol type. In 2010, the maximum density area is depicted for ($AOD_{500\ nm}$, $\alpha_{380–1020\ nm}$) = (0.39 to 0.42, 1.29 to 1.32), which also corresponds to UI aerosols.

The values of α depend strongly on the spectral range used for their determination. Hence the information contained in the $AOD_{500\ nm}$ versus $\alpha_{380–1020\ nm}$ scatter plot becomes more difficult to interpret, but the detailed spectral information given by the determination of α in different spectral band (Fig. 5) helps in determining and discriminating the aerosol types.

Variations in Spectral Curvature

The coefficients a_1 and a_2 were obtained through the application of the second-order polynomial fit in the spectral region 380–1020 nm. In general, large negative a_1 and a_2 values correspond to fine-mode aerosols, while positive a_2 and near zero or positive a_1 values are indicative of coarse-mode particles (Schuster *et al.*, 2006; Kaskaoutis *et al.*, 2007). The coefficients a_1 and a_2 (curvature in the polynomial fit) are plotted against $AOD_{500\ nm}$ for the period 2008–2010 in Figs. 6(a) and (b), respectively. As expected via the assertion of Schuster *et al.* (2006) and Kaskaoutis *et al.* (2007) the a_1 values are mostly negative, since they are similar to $-\alpha$ in cases of negligible curvature. For all the data, the positive a_1 values appear under low turbidity conditions. According to Schuster *et al.* (2006), positive a_1 values accompanied by positive curvature can be theoretically derived for very low fine fraction (0.3 or even less). According to Fig. 6(a), the range of a_1 is larger for lower $AOD_{500\ nm}$. The plot between a_2 and $AOD_{500\ nm}$ provides information on the atmospheric conditions under which α is independent from wavelength, so the spectral variation of $AOD_{500\ nm}$ can be accurately described by the simple Ångström formula. The data lying on or near the $a_2 = 0$ line belong to the Junge power-law size distribution. Based on these results it can be stated that in general, the error in using the simple linear fit becomes smaller with increasing atmospheric turbidity, especially for desert aerosol environments. The negative a_2 values are characterized by aerosol-size distributions dominated by fine-mode, while the positive curvatures indicate coarse-mode particles. Higher positive a_2 values (coarse-mode aerosols) are seen for the 2009 period as compared to 2008 and 2010. The low $AOD_{500\ nm}$ is found to associate with wide variability in a_2 values (both positive and negative), implying large curvature in Eq. (2). In contrast, for high $AOD_{500\ nm}$ a_2 tends to zero, indicating low curvature and insignificant wavelength dependence of α.

The affinity between the Ångström exponent α and the difference of a_2 and a_1 is shown in Fig. 7. According to Schuster *et al.* (2006), α is equal to the difference of a_2–a_1 to a first approximation. An attempt to verify the validity of this statement is given in Fig. 7. When the curvature is

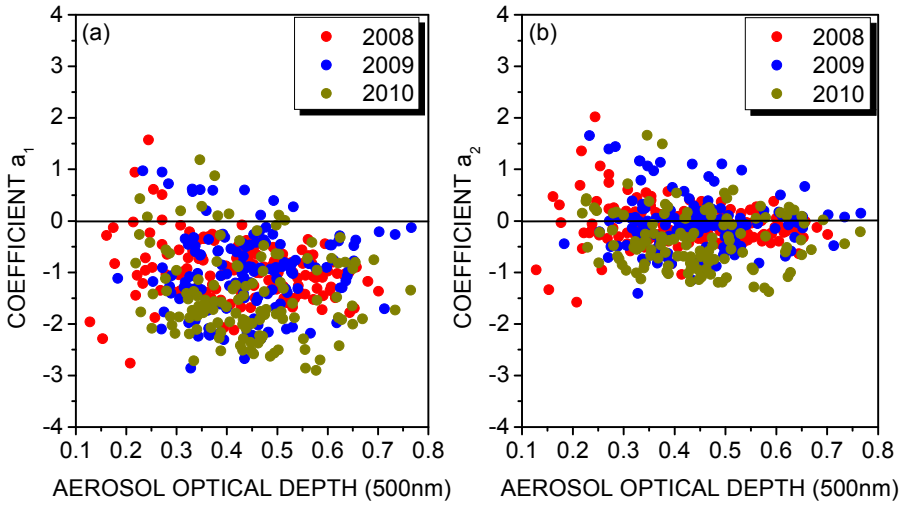

Fig. 6. Variation of the (a) coefficient a_1 against $AOD_{500\ nm}$ (b) coefficient a_2 against $AOD_{500\ nm}$ for the period 2008–2010.

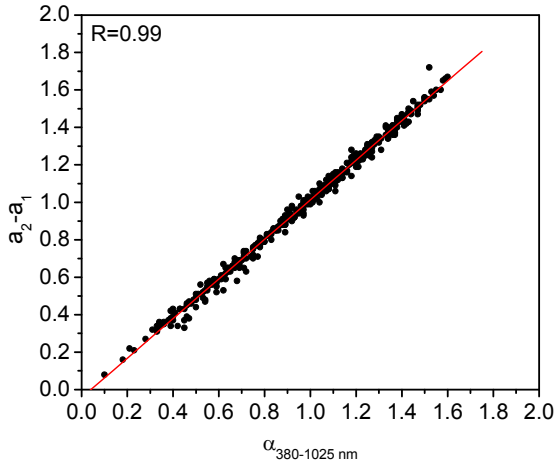

Fig. 7. Correlation between the difference (a_2 minus a_1) and $\alpha_{380–1020\ nm}$.

negligible (a_2~0), then $\alpha = -a_1$. These two parameters are strongly correlated, as indicated by the correlation coefficient of 0.99. Thus the present findings are in good agreement with those of Schuster *et al.* (2006).

Comparison between Ground-based and Satellite Observations

The correlation between the ground-based MICROTOPS-II derived AOD, PWC and TCO and those derived from MODIS and OMI satellite observations for the latitude/longitude similar to that of Pune location is depicted as a scatter plot in Fig. 8. The deviations observed in the above comparison could be due to the large variability in the column AOD, PWC and TCO at a location close to urban station. Moreover, differences in filter centre wavelengths and other optical characteristics of the instruments also lead to degrade the correlation (Bhawar and Devara, 2010). The main difficulty in satellite and ground-based measurements lies in the data sampling which leads to differences in their data structures. During its overpass, the satellite crosses a particular site instantaneously whereas the ground-based radiometer makes point measurement several times in a day. Further, the highly variable tropical climate, weather patterns, cloud conditions and local sources may play a pivotal role in the observed low correlations or the differences.

Comparison between MICROTOPS and AERONET Observations

Fig. 9 shows the comparison between Microtops and Aeronet observations at common wavelengths. The inter-comparison shows close agreement between the two measurements as indicated by the R values and the linear fit between the retrieved AOD and PWC, thus providing confidence in the operation and quality of the handheld measurements. This type of comparison helps in understanding the application of network measurements to trend studies and the ability to develop a single global climatology from multiple networks without introducing network bias.

Variations in Meteorological Parameters

Pune is about 100 km inland from the west coast of India and is located on the lee-side of the Western Ghats. The air flow in the lower troposphere is predominantly westerly during the south-west (SW) monsoon season when there is a large influx of moisture from the Arabian Sea, and an easterly flow sets in from October, and continental air masses, rich in nuclei of continental origin, pass over the station. Fig. 10 depicts monthly mean variations in temperature, relative humidity and rainfall during 2008–2010. Though the trends of variations in these parameters are more or less similar, considerable differences, particularly in the case of rainfall, are seen between the SW monsoon seasons of 2008, 2009 and 2010. The above figure shows higher temperature (less relative humidity) in 2009 as compared to 2008 and 2010. This will have an impact on formation and growth of aerosols over the experimental site during drought year 2009. Shaw *et al.* (1988) and Sharma *et al.* (2003) suggest that the size distribution of aerosols varies significantly with changes in temperature

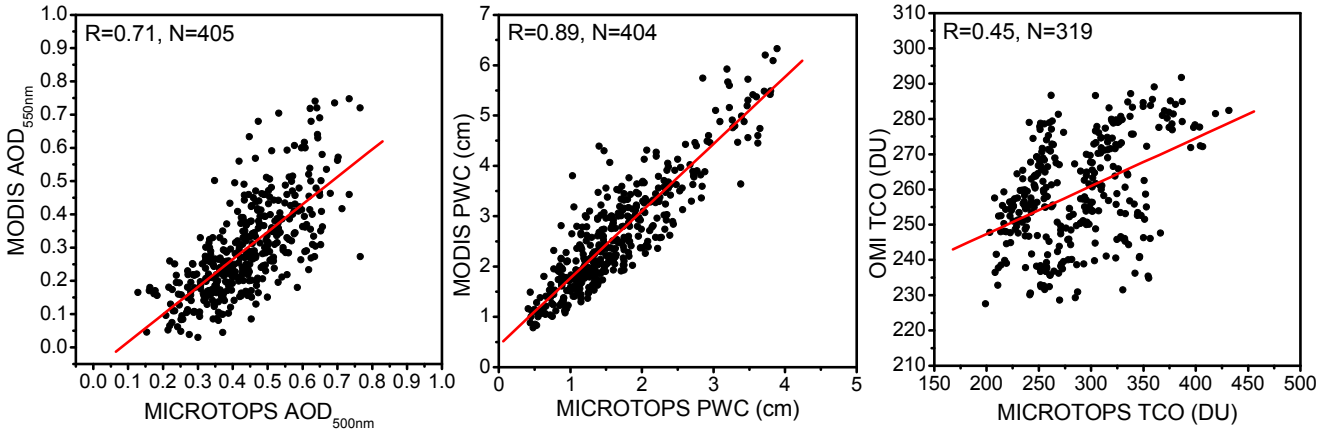

Fig. 8. Intercomparison between MICROTOPS $AOD_{500\ nm}$, PWC, TCO and MODIS $AOD_{550\ nm}$, MODIS PWC, OMI TCO.

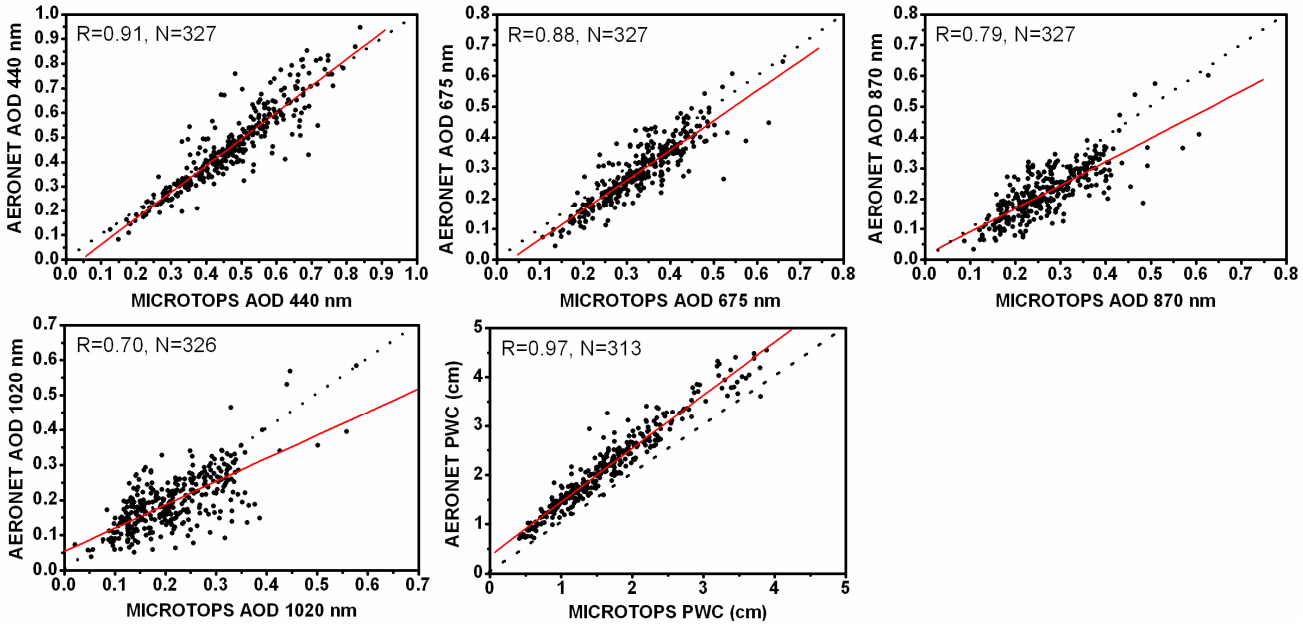

Fig. 9. The retrieved MICROTOPS AODs and PWC compared with AERONET for the wavelength of 440 nm, 675 nm, 870 nm, 1020 nm and PWC during 2008–2010. Solid and dashed lines indicate regression fit to data and 1:1 correspondence, respectively.

and relative humidity (RH). Parameswaran and Vijaykumar (1994) found that the RH does not affect significantly the aerosol concentration and size distribution up to a limit of 95%. Devara and Raj (1997) have observed that the higher RH and lower temperature during monsoon period at Pune, India, enhances the growth of cloud droplets which results in higher rainfall. Apart from the atmospheric circulation systems that favor/suppress the monsoon activity, the higher RH (lower temperature) observed during SW monsoon season of 2008 and 2010 might have assisted the cloud condensation nuclei to grow and form more cloud droplets which results in higher rainfall in those years. In 2009, during July, rainfall activity over the country as a whole was near normal. The interaction between monsoon flow and mid-latitude westerlies resulted in good rainfall activity over west and south peninsula and central parts of the country while northwestern and northeastern regions received deficient rainfall. Thus 2009 monsoon failed almost in all months, except in July. The report by the India Meteorological Department (IMD) monsoon report in 2009 pointed out that southwest monsoon season (June to September) rainfall over the whole country was deficient [(78% of its long period average (LPA)] which is the third deficient monsoon year of the decade after 2002 and 2004 (Tyagi, 2009). It also reports (Tyagi, 2008, 2010) that the rainfall for the season (June to September) for the whole country was near normal (98% of its long period average (LPA)) in 2008 and 102% of LPA in 2010. The mean intensity of rainfall does not seem to change between normal and drought years, but the variability seems to be slightly higher during a normal year. The mean seasonal rainfall, heavy/extreme rainfall, one-day maximum rainfall and rainy days associated with heavy rainfall events are significantly low during the drought year, and the seasonal rainy days

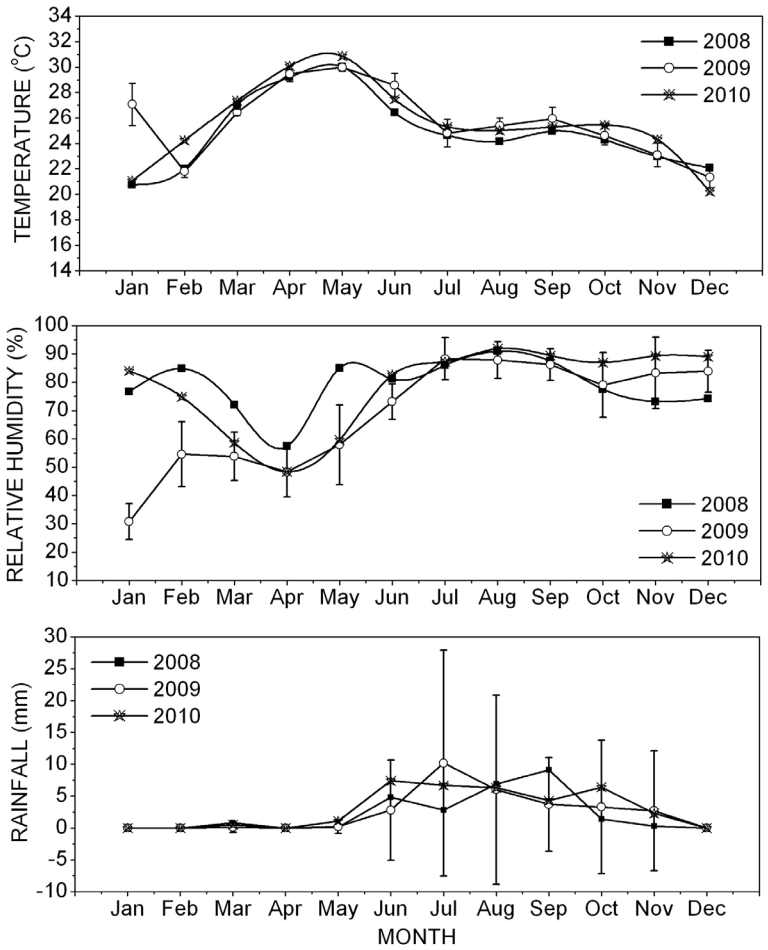

Fig. 10. Monthly mean surface-level temperature, relative humidity and rainfall during 2008–2010. Vertical bars indicate standard deviation from mean of the data for the year 2009.

also show significant low values during the drought year 2009 compared to the normal years 2008 and 2010. This indicates that a monsoon drought is associated with a drastic reduction in heavy rainfall activities compared to the normal monsoon year.

Inferences from TRMM Observations

Fig. 11 shows monsoon rain rate over the Indian region during 2008–2010 derived from TRMM. These figures clearly show that, less amount of rainfall was observed over the Indian region during 2009. In 2009, an increase of aerosol optical depth (AOD) causes increase in shallow cloud cover, decrease in cloud droplet size, and reduction/ delay of the rainfall formation. This is consistent with the results reported by Kaufman and Nakajima (1993). Enhancement in AOD, larger values of alpha and increase in temperature indicate more contribution of fine (soil-dust) particles to the cloud formation during pre-monsoon season of 2009. These particles (act as CCN under favorable meteorological conditions) eventually help in the formation of clouds dominated by small droplets but with low coalescence efficiencies (Rosenfeld *et al.*, 2001). Such situation suppresses rainfall because rain formation/ development needs the presence of both smaller and larger droplets.

One of the most prominent features of the tropical oceans is the existence of warm pools (region with temperature greater than 28°C). They exhibit important implications to atmospheric processes, particularly during the onset phase of Indian summer monsoon and associated precipitation characteristics. Tropical warm pools appear as the primary mode in the distribution of tropical sea surface temperature (SST). It has been shown that the minimum SST required for active convection is 28°C (Gadgil *et al.*, 1984; Graham and Barnet, 1987). It has also been found that regions with annual mean SST above 28°C are prone to tropical cyclones (Gray, 1975). Fig. 12 shows the annual mean of SST over the Indian region during 2008–2010. These figures clearly indicate higher SST during 2009 compared to 2008 and 2010. The extent and intensity of warm pool depend on the type of monsoon. Maximum core temperature and wide coverage of warm pool occur during the excess monsoon years compared to normal and deficient monsoon years (Deepa *et al.*, 2010; Neema *et al.*, 2011).

The location and regional extent of the warm pool in the Arabian Sea were distinct during the period of study. In 2009, the warm pool core was located in the equatorial region, whereas in 2010, it spreads to a wide region of the

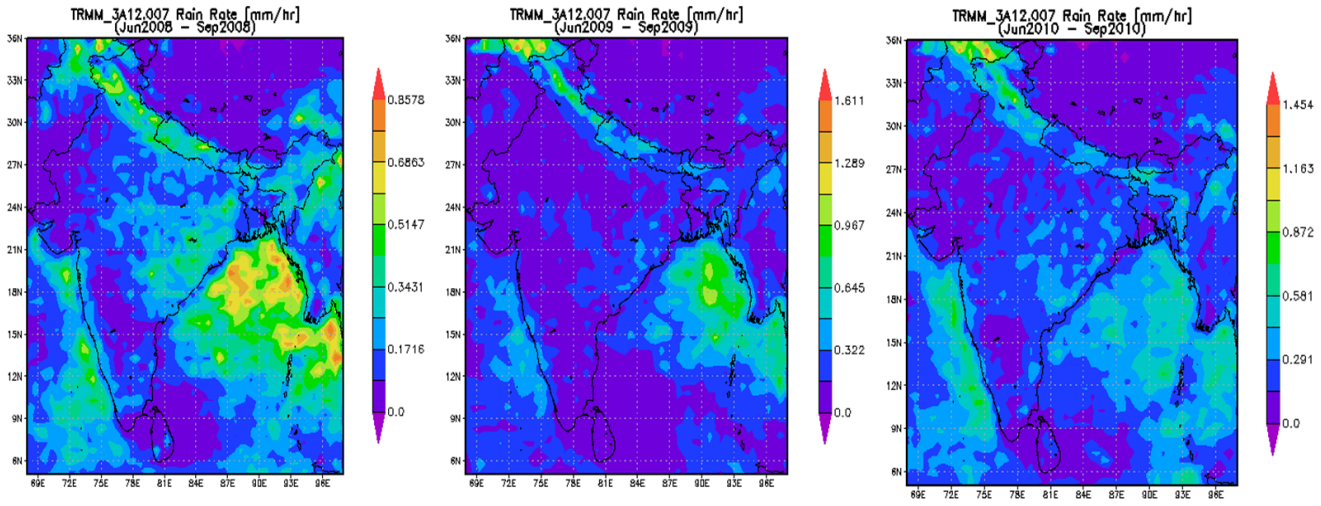

Fig. 11. Rain rate over the Indian region during monsoon months (June–September) from 2008 to 2010, derived from TRMM.

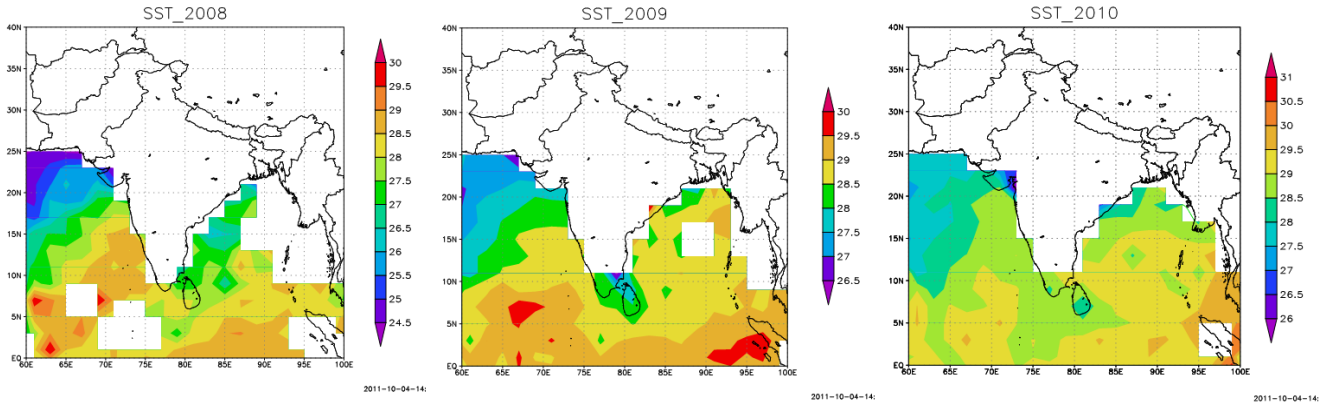

Fig. 12. Annual mean of SST over the Indian region during 2008–2010.

Arabian Sea (AS). The results of a recent study reported by Sijikumar and Rajeev (2012) indicated suppressed convection over the central and northern AS in 2009 while warmer SSTs in the AS favor enhanced convection during 2010 combined with a sharp contrast in the moisture transport. SST is also important because the properties of the surface and mixed layer air are closely linked to the SST, due to continuous interactions of the upper layer of the ocean and the atmosphere immediately above (Bhat *et al.*, 1996). When the atmosphere is free from clouds, the ocean surface receives net heat, SST increases, enhancing the energy of the surface air as well. Gadgil *et al.* (1984) concluded that over the Indian Ocean, 28°C is the threshold for deep convection. When deep convection occurs, the clouds block solar radiation and latent heat flux increases due to increased winds. Hence the ocean cools. This can lead to reduced convection. Thus, whereas atmospheric convection depends upon the SST, the SST changes in response to atmospheric convection and the system is coupled. Therefore, understanding of the annual variation of SST over the Indian region is important in the studies related to monsoon onset over Kerala and maintenance of the West coast monsoon.

CONCLUSIONS

- On the basis of the sunphotometer data, AOD values at all wavelengths are found to be high during 2009 compared to 2008 and 2010, suggesting an additional loading of aerosols over the region.
- The column PWC is observed to be smaller during 2009 in contrast to that during 2008 and 2010.
- Both OMI and MICROTOPS-II exhibit lower ozone values during winter and pre-monsoon seasons and higher values during monsoon and post-monsoon seasons of 2008–2010.
- The case of negative curvature ($a_2 < 0$) is characteristic of aerosol size distribution dominated by fine-mode particles while the case of positive curvature ($a_2 > 0$) denotes size distribution dominated by coarse-mode aerosols. The latter dominates during 2009 compared to 2008 and 2010.
- The ground-based observations from MICROTOPS-II reveal good correlation with satellite and AERONET observations, thus providing confidence in the operation and quality of the handheld measurements.
- The discrimination of aerosol type over Pune reveals

maximum UI aerosols in 2009 and minimum in 2008 and 2010.

- ❖ Higher temperatures observed in 2009, as compared to 2008 and 2010; suppress the formation and growth of aerosols over the experimental site during bad monsoon year 2009. In contrast, higher RH and lower temperature during active monsoon years 2008 and 2010 are found to favor the growth of cloud droplets, resulted in higher rainfall.

ACKNOWLEDGEMENTS

We are grateful to the Editor and anonymous reviewers for their valuable suggestions and useful comments on the original manuscript. Thanks are due to the Director, IITM for encouragement and support. The meteorological data support from the India Meteorological Department, Pune, is acknowledged with thanks. We thank NCEP/NCAR reanalysis data obtained from NOAA-CIRES Climate Diagnostic Center, Boulder, Colorado from their website http://www.cdc.noaa.gov. The financial support from ISRO-GBP-ARFI and SAC-ISRO is gratefully acknowledged.

REFERENCES

Ångström, A. (1964). The Parameters of Atmospheric Turbidity. *Tellus* 16: 64–75.

Badarinath, K.V.S., Shailesh Kumar, K., Madhavi Latha, K., Kiran Chand, T.R., Krishna Prasad, V., Nirmala Jyothsna, A. and Samatha, K. (2007a). Multiyear Ground-Based and Satellite Observations of Aerosol Properties over a Tropical Urban Area in India. *Atmos. Sci. Lett.* 8: 7–13.

Badarinath, K.V.S., Shailesh Kumar, K., Kaskaoutis, D.G. and Kambezidis, H.D. (2007b). Influence of Atmospheric Aerosols on Solar Spectral Irradiance in an Urban Area. *J. Atmos. Sol. Terr. Phys.* 69: 589–599.

Bao, Z., Zhu, C., Hulugalla, R., Gu, J. and Di, G. (2008). Spatial and Temporal Characteristics of Aerosol Optical Depth over East Asia and Their Association with Wind Fields. *Meteorol. Appl.* 15: 455–463

Bellouin, N., Boucher, O., Haywood, J. and Reddy, M.S. (2005). Global Estimate of Aerosol Direct Radiative Forcing from Satellite Measurements. *Nature* 438: 1138–1141.

Bhat, G.S., Srinivasan, J. and Gadgil, S. (1996). Tropical Deep Convection, Convective Available Potential Energy and Sea Surface Temperature. *J. Meteorol. Soc. Jpn.* 74: 155–166.

Bhawar, R.L. (2008). Aerosol Characterization from Satellite and Ground-Based Measurements, Ph.D Thesis, University of Pune.

Bhawar, R.L. and Devara, P.C.S. (2010). Study of Successive Contrasting Monsoons (2001-2002) in Terms of Aerosol Variability over a Tropical Station Pune, India. Atmos. Chem. *Phys*. 10: 29–37.

Chu, D.A., Kaufman, Y.J., Ichoku, C., Remer, L.A., Tanré, D. and Holben, B.N. (2002). Validation of MODIS Aerosol Optical Depth Retrieval over Land. *Geophys. Res. Lett.* 29: 8007, doi: 10.1029/2001GL013205.

Dani, K.K., Raj, P.E, Devara, P.C.S., Pandithurai, G., Sonbawne, S.M., Maheskumar, R.S., Saha, S.K. and Jaya Rao, Y. (2010). Long-Term Trends and Variability in Measured Multi-Spectral Aerosol Optical Depth over a Tropical Urban Station in India. *Int. J. Climatol.* 32: 153–160.

Deepa, R., Gnanaseelan, C., Seetaramayya, P. and Nagar, S.G. (2010). On the Relationship between Arabian Sea Warm Pool and Formation of Onset Vortex over East-Central Arabian Sea. *Meteorol. Atmos. Phys.* 108: 113–125.

Devara, P.C.S., Raj, P.E., Sharma, S. and Pandithurai, G. (1994). Lidar Observed Long-Term Variations in Urban Aerosol Characteristics and Their Connection with Meteorological Parameters. *Int. J. Climatol.* 14, 581–592.

Devara, P.C.S. and Raj, P.E. (1997). A Lidar Study of Atmospheric Aerosols during Two Contrasting Monsoon Season. *Atmosfera* 11: 199–204.

Devara, P.C.S, Maheskumar, R.S, Raj, P.E., Dani, K.K. and Sonbawne, S.M. (2001). Some Features of Columnar Aerosol Optical Depth, Ozone and Precipitable Water Content Observed Over Land during the INDOEX-IFP99. *Meteorol. Z.* 10: 123–130.

Devara, P.C.S., Maheskumar, R.S., Raj, P.E., Pandithurai, G. and Dani, K.K. (2002). Recent Trends in Aerosol Climatology and Air Pollution as Inferred from Multi-Year Lidar Observations over a Tropical Urban Station. *Int. J. Climatol.* 22: 435–449.

Eck, T.F., Holben, B.N., Reid, J.S., Dubovik, O., Smirnov, A., O'Neill, N.T., Slutsker, I. and Kinne, S. (1999). Wavelength Dependence of the Optical Depth of Biomass Burning, Urban, and Desert Dust Aerosols. *J. Geophys. Res.* 104: 31333–31349.

Eck, T.F., Holben, B.N., Dubovic, O., Smirnov, A., Slutsker, I., Lobert, J.M. and Ramanathan, V. (2001a). Column-Integrated Aerosol Optical Properties over the Maldives during the Northeast Monsoon for 1998–2000. *J. Geophys. Res.* 106: 28555–28566.

Eck, T.F., Holben, B.N., Ward, D.E., Dubovic, O., Reid, J.S., Smirnov, A., Mukelabai, M.M., Hsu, N.C., O'Neil, N.T. and Slutsker, I. (2001b). Characterization of the Optical Properties of Biomass Burning Aerosols in Zambia during the 1997 ZIBBEE Field Campaign. *J. Geophys. Res.* 106: 3425–3448.

Gadgil, S., Joshi, N.V. and Joseph, P.V. (1984). Ocean-Atmosphere Coupling over Monsoon Regions. *Nature* 312: 141–143.

Graham, N.E. and Barnet, T.P. (1987). Sea Surface Temperature, Surface Wind Divergence and Convection over Tropical Oceans. *Science* 238: 657–659.

Gray, W.M. (1975). *Tropical Cyclone Genesis*. Dept Atmos. Sci., Paper. 232, Colorado State University, Ft. Colins, Co, 121 pp.

Gupta, P., Gadhavi, H. and Jayaraman, A. (2003). Aerosol Optical Depth Variation Observed Using Sunphotometer over Indore. *Indian J. Radio Space Phys.* 32: 229–237.

Haywood, J. and Boucher, O. (2000). Estimates of the Direct and Indirect Radiative Forcing due to Tropospheric

Aerosols. *Rev. Geophys.* 38: 513–543.

Holben, B.N., Eck, T.F., Slutsker, I., Tanré, D., Buis, J.P., Setzer, A., Vermote, E., Reagan, J.A., Kaufman, Y.J., Nakajima, T., Lavenu, F., Jankowiak, I. and Smirnov, A. (1998). AERONET - A Federated Instrument Network and Data Archive for Aerosol Characterization. *Remote Sens. Environ.* 66: 1–16.

Holben., B.N., Tanré, D., Smirnov, A., Eck, T.F., Slutsker, I., Abuhasaan, N., Kaufman, Y.J., Vande Castle, J., Setzer, A., Markham, B., Clark, D., Frouin, R., Halthore, R., Karneli, A., O'Neill, N.T., Pietras, C., Pinker, R.T., Voss, K. and Zibordi, G. (2001). An Emerging Ground-Based Aerosol Climatology: Aerosol Optical Depth from AERONET. *J. Geophys. Res.* 106: 12067–12097.

Ichoku, C., Chu, D.A., Matoo, S., Kaufman, Y.J., Remer, L.A. and Tanré, D. (2002). A Spatio-Temporal Approach for Global Validation and Analysis of MODIS Aerosol Products. *Geophys. Res. Lett.* 29: 8006, doi: 10.1029/2001GL013206.

Kalapureddy, M.C.R. and Devara, P.C.S. (2008). Characterization of Aerosols over Oceanic Regions around India during Pre-Monsoon 2006. *Atmos. Environ.* 42: 6816–6827.

Kaskaoutis, D.G. and Kambezidis, H.D. (2006). Investigation into the Wavelength Dependence of the Aerosol Optical Depth in the Athens Area. *Q. J. R. Meteorolog. Soc.* 132: 2217–2234.

Kaskaoutis, D.G., Kambezidis, H.D., Adamopoulos, A.D. and Kassomenos, P.A. (2006). Comparison between Experimental Data and Modeling Estimates of Atmospheric Optical Depth over Athens, Greece. *J. Atmos. Sol. Terr. Phys.* 68: 1167–1178.

Kaskaoutis, D.G., Kambezidis, H.D., Hatzianastassiou, N., Kosmopoulos, P.G. and Badarinath, K.V.S. (2007). Aerosol Climatology: Dependence of the Ångström Exponent on Wavelength over Four AERONET Sites. *Atmos. Chem. Phys. Discuss.* 7: 7347–7397.

Kaskaoutis, D.G. and Kambezidis, H.D. (2008). Comparison of the Ångström Parameters Retrieval in Different Spectral Ranges with the Use of Different Techniques. *Meteorol. Atmos. Phys.* 99: 233–246.

Kaskaoutis, D.G., Badarinath, K.V.S., Kharol, S.K., Sharma, A.R. and Kambezidis, H.D. (2009). Variations in the Aerosol Optical Properties and Types over the Tropical Urban Site of Hyderabad, India. *J. Geophys. Res.* 114: D22204, doi: 10.1029/2009JD012423.

Kasten, F. and Young, A.T. (1989). Revised Optical Air Mass Tables and Approximation Formula. *Appl. Opt.* 28: 4735–4738.

Kaufman, Y.J. and Nakajima, T. (1993). Effect of Amazon Smoke on Cloud Microphysics and Albedo-Analysis from Satellite Imagery. *J. Appl. Meteorol.* 32: 729–744.

Kaufman, Y.J., Tanré, D., Remer, L.A., Vermote, E.F., Chu, A. and Holben, B.N. (1997). Operational Remote Sensing of Tropospheric Aerosol over Land from EOS Moderate Resolution Imaging Spectroradiometer. *J. Geophys. Res.* 102: 17051–17067.

Kaufman, Y.J., Remer, L.A., Tanré, D., R-Li, R., Kleidman, R., Mattoo, S., Levy, R.C., Eck, T.F., Holben, B.N., Ichoku, C., Martins, V.J. and Koren, I. (2005). A Critical Examination of the Residual Cloud Contamination and Diurnal Sampling Effects on MODIS Estimates of Aerosol over Ocean. *IEEE Trans. Geosci. Remote Sens.* 43: 2886–2897.

Khemani, K.T., Momin, G.A., Naik, M.S., Rao, P.S.P., Kumar, R. and Ramana Murty, Bh.V. (1985). Trace Elements and Sea Salt Aerosols over the Sea Areas around the Indian Sub-Continent. *Atmos. Environ.* 19: 277–284.

Khemani, L.T., Momin, G.A., Naik, M.S., Vijayakumar, R. and Ramana Murthy, Bh.V. (1982). Chemical Composition and Size Distribution of Atmospheric Aerosols over the Deccan Plateau, India. *Tellus* 34: 151–158.

Khemani, L.T. (1989). Physical and Chemical Characteristics of Atmospheric Aerosols. In *Air Pollution Control*, Vol. 2, Cherimisinoff, P.N. (Ed.), Encyclopedia of Environmental Control Technology, Gulf Publ. Co., USA, p. 401–452.

Kim, D.H., Sohn, B.J., Nakajima, T., Takamura, T., Takemura, T., Choi, B.C. and Yoon, S.C. (2004). Aerosol Optical Properties over East Asia Determined from Ground-Based Sky Radiation Measurements. *J. Geophys. Res.* 109: D02209, doi: 10.1029/2003JD003387.

Levy, R.C., Remer, L.A., Mattoo, S., Vermote, E. and Kaufman, Y.J. (2007). Second Generation Operational Algorithm: Retrieval of Aerosol Properties over Land from Inversion of Moderate Resolution Imaging Spectroradiometer Spectral Reflectance. *J. Geophys. Res.* 112: D13211, doi: 10.1029/2006JD007811.

Li, F. and Ramanathan, V. (2002). Winter to Summer Monsoon Variation of Aerosol Optical Depth over the Tropical Indian Ocean. *J. Geophys. Res.* 107: 4284, doi: 10.1029/2001JD000949.

Masmoudi, M., Chaabane, M., Tanré, D., Gouloup, P., Blarel, L. and Elleuch, F. (2003). Spatial and Temporal Variability of Aerosol: Size Distribution and Optical Properties. *Atmos. Res.* 66: 1–19.

Moorthy, K.K., Satheesh, S.K., Babu, S.S. and Dutt, C.B.S. (2008). Integrated Campaign for Aerosols, Gases and Radiation Budget (ICARB): An Overview. *J. Earth Syst. Sci.* 117: 243–262.

Morys, M., Mims, F.M., Hagerup, S., Anderson, S.E., Baker, A., Kia, J. and Walkup, T. (2001). Design, Calibration, and Performance of MICROTOPS-II Handled Ozone Monitor and Sun Photometer. *J. Geophys. Res*. 106: 14573–14582.

Neema, C.P., Hareeshkumar, P.V. and Babu, C.A. (2011). Characteristics of Arabian Sea Mini Warm Pool and Indian Summer Monsoon. *Clim. Dyn.* 38: 2073–2087.

Pace, G., di Sarra, A., Meloni, D., Piacentino, S. and Chamard, P. (2006). Aerosol Optical Properties at Lambeduca (Central Mediterranean), 1. Influence of Transport and Identification of Different Aerosol Types. *Atmos. Chem. Phys.* 6: 697–713.

Pandey, R. and Vyas, B.M. (2004). Study of Total Column Ozone, Precipitable Water Content and Aerosol Optical Depth at Udaipur, a Tropical Station. *Curr. Sci.* 86: 305–309.

Parameswaran, K. and Vijaykumar, G. (1994). Effect of Atmospheric Relative Humidity on Aerosol Size

Distribution. *Indian J. Radio Space Phys.* 23: 175–178.

Pedros, R., Martinez-Lozano, J.A., Utrillas, M.P., Gomez-Amo, J.L. and Tena, F. (2003). Column-Integrated Aerosol, Optical Properties from Ground-based Spectroradiometer Measurements at Barrax (Spain) During the Digital Airborne Imaging Spectrometer Experiment (DAISEX) Campaigns. *J. Geophys. Res.* 108: 4571, doi: 10.1029/2002JD003331.

Praveen, P.S. (2008). *Aerosol Properties in Different Environments*, Ph.D. Thesis, University of Pune, Pune, India, p. 170.

Rahul, P.R.C., Salvekar, P.S and Devara, P.C.S. (2008). Aerosol Optical Depth Variability over Arabian Sea during Drought and Normal years of Indian Monsoon. *Geophys. Res. Lett*. 35: L22812, doi: 10.1029/2008GL035573.

Raj, P.E. and Devara, P.C.S. (1989). Some Results of Lidar Aerosol Measurements and Their Relationship with Meteorological Parameters. *Atmos. Environ.* 23:831–838.

Raj, P.E., Devara, P.C.S., Maheskumar, R.S., Pandithurai, G., Dani, K.K., Saha, S.K., Sonbawne, S.M. and Tiwari, Y.K. (2004). Results of Sun Photometer-Derived Precipitable Water Content over a Tropical Indian Station. *J. Appl. Meteorol*. 43: 1452–1459.

Raj, P.E., Devara, P.C.S., Saha, S.K., Sonbawne, S.M., Dani, K.K., Pandithurai, G. and Ramana Murthy, A. (2008). Temporal Variations in Sun Photometer Measured Precipitable Water in Near IR Band and Its Comparison with Model Estimates at a Tropical Indian Station. *Atmosfera* 21: 317–333.

Raj, P.E., Sonbawne, S.M., Dani, K.K., Saha, S.K., Pandithurai, G. and Devara, P.C.S. (2009). Changes Observed in Sun Photometer Derived Total Column Ozone and Possible Implications on Surface-Reaching UV Radiation over a Tropical Indian Station. *Int. J. Remote Sens*. 30: 4153–4165.

Ranjan, R.R., Ganguly D.N., Joshi, H.P. and Iyer, K.N. (2007). Study of Aerosol Optical Depth and Precipitable Water Vapor Content at Rajkot, a Tropical Semi – Arid Station. *Indian J. Radio Space Phys.* 36: 27–32.

Rawlins, M.A., Serreze, M.C., Schroeder, R., Zhang, X. and McDonald, K.C. (2009). Diagnosis of the Record Discharge of Arctic- Draining Eurasian Rivers in 2007. *Environ. Res. Lett.* 4: 045011, doi: 10.1088/1748-9326/4/4/045011.

Remer, L.A. (2005). The MODIS Aerosol Algorithm, Products, and Validation. *J. Atmos. Sci.* 62: 947–973.

Rosenfeld, D., Rudich, Y. and Lahav, R. (2001). Desert Dust Suppressing Precipitation: A Possible Desertification Feedback Loop. *Proc. Nat. Acad. Sci. U.S.A.* 98: 5975–5980.

Rosenfeld, D. (2006). Aerosols, Clouds and Climate. *Science* 312: 1323–1324.

Satheesh, S.K., Ramanthan, V., Holben, B.N., Moorthy, K.K., Loeb, N.G., Maring, H., Prospero, J.M. and Savoie, D. (2002). Chemical, Microphysical and Radiative Effects of Indian Ocean Aerosols. *J. Geophys. Res.* 107: 4725, doi: 10.1029/2002JD002463.

Schuster, G.L., Dubovik, O. and Holben, B.N. (2006). Ångström Exponent and Bimodal Aerosol Size Distributions. *J. Geophys. Res.* 111: D07207, doi: 10.1029/2005JD006328.

Sharma, D.K., Rai, J., Israil, M. and Singh, P. (2003). Summer Variations of the Atmospheric Aerosol Number Concentration over Roorkee, India. *J. Atmos. Sol. Terr. Phys.* 65:1007–1019.

Shaw, G.E. (1988). Aerosol-Size Temperature Relationship. *Geophys. Res. Lett.* 15: 133–135.

Shettle, E.P. and Fenn, R.W. (1979). Models for the Aerosols of the Lower Atmosphere and the Effects of Humidity Variations on their Optical Properties. *Air Force Geophysics Laboratory Tech. Rep.* AFGL-TR-79-0214, p. 94.

Sijikumar, S. and Rajeev, K. (2012). Role of the Arabian Sea Warm Pool on the Precipitation Characteristics during the Monsoon Onset Period. *J. Climate* 25: 1890–1899.

Smirnov, A., Holben, B.N., Eck, T.F., Dubovik, O. and Slutsker, I. (2000). Cloud Screening and Quality Control Algorithms for the AERONET Data Base. *Remote Sens. Environ*. 73: 337–349.

Sumit, K., Devara, P.C.S., Dani, K.K., Sonbawne, S.M. and Saha, S.K. (2011). Sun-Sky Radiometer–Derived Column-Integrated Aerosol Optical and Physical Properties over a Tropical Urban Station during 2004–2009. *J. Geophys. Res.* 116: D10201, doi: 10.1029/2010JD014944.

Tanré, D., Kaufman, Y.J., Herman, M. and Mattoo, S. (1997). Remote Sensing of Aerosol Properties over Oceans using the MODIS/EOS Spectral Radiances. *J. Geophys. Res.* 102: 16971–16988.

Tyagi, A., Hatwar, H.R. and Pai, D.S. (2009). Monsoon 2008 - A Report, IMD Met Monograph/Synoptic Meteorology No: 7/2009.

Tyagi A., Hatwar, H.R. and Pai, D.S. (2010). Monsoon 2009 - A Report, IMD Met Monograph/Synoptic Meteorology No: 9/2010.

Tyagi A., Mujundar, A.B. and Pai, D.S. (2011). Monsoon 2010 - A Report, IMD Met Monograph/Synoptic Meteorology No: 10/2011.

Wang, B. (2006). *The Asian Monsoon*, Springer and Praxis, 787 pp.

WMO (World Meteorological Organization) (2003). *Scientific Assessment of Ozone Depletion: 2002*, Global Ozone Research and Monitoring Project - Report No. 47, 498 pp., Geneva.

Received for review, January 5, 2012
Accepted, May 26, 2012